J. Fluid Mech. (1987), *vol.* 174, *pp.* 209–231
Printed in Great Britain

Heat-flow experiments in liquid ^{4}He with a variable cylindrical geometry

By H. GAO, G. METCALFE, T. JUNG† AND R. P. BEHRINGER
Duke University, Durham, NC 27706, USA

(Received 2 July 1985 and in revised form 12 March 1986)

This paper first describes an apparatus for measuring the Nusselt number N versus the Rayleigh number R of convecting normal liquid ^{4}He layers. The most important feature of the apparatus is its ability to provide layers of different heights d, and hence different aspect ratios Γ. The horizontal cross-section of each layer is circular, and Γ is defined by $\Gamma = D/2d$ where D is the diameter of the layer. We report results for $2.4 \leqslant \Gamma \leqslant 16$ and for Prandtl numbers Pr spanning $0.5 \lesssim Pr \lesssim 0.9$. These results are presented in terms of the slope $N_1 = R_c dN/dR$ evaluated just above the onset of convection at R_c. We find that N_1 is only a slowly increasing function of Γ in the range $6 \lesssim \Gamma \lesssim 16$, and that it has a value there which is quite close to 0.72. This value of N_1 is in good agreement with variational calculations by Ahlers *et al.* (1981) pertinent to parallel convection rolls in cylindrical geometry. Particularly for $\Gamma \lesssim 6$, we find additional small-scale structure in N_1 associated with changes in the number of convection rolls with changing Γ. An additional test of the linearized hydrodynamics is given by measurements of R_c. We find good agreement between theory and our data for R_c.

1. Introduction

Work on nonlinear systems has stimulated current interest in Rayleigh–Bénard convection. Several authors including Libchaber & Maurer (1978, 1980), Maurer & Libchaber (1979, 1980); Ahlers (1980); Ahlers & Walden (1980); Behringer *et al.* (1982); and Ahlers & Behringer (1978*a*, *b*) have shown that the aspect ratio Γ significantly affects convective flows. By Γ we mean the characteristic horizontal length of the layer expressed in units of its height d. In order to better understand these observations, we constructed an apparatus which allows us to vary Γ continuously and *in situ*. The apparatus has a circular cross-section, and the aspect ratio is defined by

$$\Gamma = \frac{D}{2d}, \tag{1}$$

where D is the diameter. In this paper, we characterize the steady convective flows preceding turbulence by presenting precise measurements of the heat transport as a function of the Rayleigh number R. These measurements cover the range $2.4 \leqslant \Gamma \lesssim 16$. An important feature of these experiments is that they provide an extensive set of cryogenic measurements which both spans a large range of aspect ratios and has uniform experimental conditions. We present our results in terms of the Nusselt number N, a dimensionless measure of the heat transport formed by the

† Present address: Department of Physics, University of Maryland, College Park, MD 20742, USA.

ratio of the heat flux traversing the layer to the heat flux that would be needed to sustain the same temperature difference across the layer in the absence of convection. We discuss these measurements in the light of recent calculations (Charlson & Sani 1975; Brown & Stewartson 1978, 1979; Ahlers *et al.* 1981) which relate the flow pattern formed by the convection rolls, confined in a cylindrical container, to the Nusselt number. The present data form a background for extensive studies of time-dependent flows that have been obtained using this apparatus and that have been briefly discussed elsewhere (Behringer, Gao & Shaumeyer 1983; Gao & Behringer 1984). Part 2 of this work (which is in preparation) will describe the time-dependent states in detail.

Three parameters are needed to describe the state of the convective flow; these are Γ, R and the Prandtl number Pr. The Rayleigh number is defined conventionally as

$$R = \frac{\alpha_p g d^3 \Delta T}{\kappa \nu}, \tag{2}$$

where the fluid parameters α_p, ν and κ are respectively the isobaric expansion coefficient, the kinematic viscosity and the thermal diffusivity. Additionally, ΔT is the temperature difference across the layer, and g is the acceleration due to gravity. The Prandtl number is defined as

$$Pr = \frac{\nu}{\kappa}. \tag{3}$$

Liquid ^{4}He in the normal phase forms the operating fluid for these experiments, and the Prandtl numbers studied all lie in the range $0.5 \lesssim Pr \leqslant 0.9$. The advantages to be gained by using cryogenic techniques to study convection have been discussed by Ahlers (1974, 1975), Behringer & Ahlers (1982) and by Behringer (1985).

For $R \geqslant R_c$, with R_c corresponding to the onset of convection, N is expected to increase linearly with R, and a useful parameter is the slope

$$N_1 = R_c \frac{\mathrm{d}N}{\mathrm{d}R} \tag{4}$$

evaluated for R just above R_c. Our primary results are values of N_1.

Of particular relevance to this work are calculations by Charlson & Sani (1975) giving the finite-amplitude axisymmetric convective flows in low-aspect-ratio cylindrical containers, as well as analysis by Brown & Stewartson (1978, 1979) and by Ahlers *et al.* (1981) pertaining to large but finite cylindrical containers. The aspect-ratio range of the present experiments extends from the region considered by Charlson & Sani (1975) to that considered by Brown & Stewartson (1979) and by Ahlers *et al.* (1981). In addition Schlüter, Lortz & Busse (1965) have considered a horizontally infinite layer and calculated N_1 for flow patterns consisting of straight rolls, hexagons and squares. For straight parallel rolls, these authors predict a slope $N_{1\infty}$ given by

$$N_{1\infty} = g^{-1} = (0.69942 - 0.00472 Pr^{-1} + 0.00832 Pr^{-2})^{-1}. \tag{5}$$

Also useful are calculations by Clever & Busse (1974) which give N as a function of Pr and R for several convection-roll wavevectors α. These calculations pertain to a horizontally infinite layer of straight parallel rolls with a spatial periodicity $2\pi d/\alpha$.

Charlson & Sani (1975) examined the extreme cases of conducting and insulating sidewalls and a variety of Prandtl numbers. Their studies for $Pr = 1$ corresponds best to the Prandtl numbers in our experiments. Values of Γ studied by Charlson & Sani

which fall within or near our experimental range are $\Gamma = 1.00$, 2.25 (insulating sidewalls) and 2.55, 2.66 (conducting sidewalls). For the first boundary condition, the calculated values of N_1 are 0.26 and 0.37 for the respective aspect ratios $\Gamma = 1.00$ and 2.25. However, when the walls are conducting, N_1 depends strongly on the direction of flow and whether N is evaluated at the top or the bottom of the layer. For conducting walls and N_1 evaluated at the bottom of layer the calculated value of N_1 is 0.53 for $\Gamma = 2.55$, and 0.46 for $\Gamma = 2.66$. In the present experiments the sidewalls contribute approximately one quarter of the total heat flux, and therefore they correspond more closely to insulating than conducting sidewalls.

Charlson & Sani found that the axisymmetric solutions may be unstable to non-axisymmetric modes for R greater than about $1.04R_c$ to $1.1R_c$, depending on Pr and Γ, although their tests of stability to non-axisymmetric disturbances were only made for conducting sidewalls. Also, Cross (1982) has concluded that parallel rolls will be preferred over axisymmetric rolls in a cylindrical container. In this regard, experiments in cylindrical containers by Stork & Müller (1975), Kirchartz *et al.* (1981), Steinberg, Ahlers & Cannell (1984), Croquette, Mory & Schosseler (1983), Ahlers, Cannell & Steinberg (1985), Heutmaker, Fraenkel & Gollub (1985) and Pocheau, Croquette & Le Gal (1985) show non-axisymmetric roll patterns in cylindrical containers in the absence of strong perturbations at the sidewalls to enforce the axisymmetry. In particular, Pocheau *et al.* (1985) find nearly parallel rolls for R close to R_c in an experiment using argon gas ($Pr = 0.69$) in a cylindrical container with $\Gamma = 7.66$. These observations should be contrasted to older results (for instance Hoard, Robertson & Acrivos 1970; Koschmieder & Pallas 1974; Somerscales & Dougherty 1970) in which axisymmetric flows were observed. The more recent work indicates that axisymmetric states occur when there is thermal forcing at the sidewalls, either by some steady perturbation (Croquette *et al.* 1983) or by dynamic forcing (Steinberg *et al.* 1984).

Ahlers *et al.* (1981) have considered the effect of the sidewalls on several different flow patterns within a cylindrical geometry. Of interest here are axisymmetric flows with and without a central node in the flow amplitude, and cylindrically confined straight parallel rolls. Each of these cases was treated differently by the above authors; here, it is useful to briefly summarize their approach and results for the three cases.

(*a*) *Axisymmetric with central node.* The authors carried out the most extensive study for this case. Very close to the onset of convection, when only one mode is relevant, they find

$$N_1 = \frac{(1+\epsilon_c)\,N_{1\infty}}{1.6595}, \tag{6}$$

where

$$\epsilon_c = \frac{\pi^2 \xi_0^2}{\Gamma^2} \tag{7}$$

and $\xi_0^2 = 0.148$ for the rigid non-slip horizontal walls considered here. Also, $N_{1\infty}$ is given in (5). As ϵ, defined in terms of the aspect-ratio-dependent critical Rayleigh number R_c by

$$\epsilon = \frac{R - R_c}{R_c} \tag{8}$$

increases above ϵ_c, a multi-mode description becomes necessary. With the addition of more modes, the authors find an upward curvature in $N(\epsilon)$.

(*b*) *Parallel rolls.* In this case, the authors used a trial function corresponding to

parallel rolls in a cylindrical geometry in a variational procedure to obtain N. The result,

$$\frac{(N-1)R}{R_c} = \frac{\epsilon(1+\bar{\epsilon}_c)}{1.38} \tag{9}$$

with

$$\bar{\epsilon}_c = \frac{1.18\pi^2\xi_0^2}{4\Gamma^2}, \tag{10}$$

does not contain the higher-order effects considered in the previous case. For large Γ, the slope is then $N_1 = (1.38)^{-1} = 0.72$.

(*c*) *Axisymmetric with finite centre amplitude.* In this case, Ahlers *et al.* (1981) refer to the earlier work by Brown & Stewartson (1979). These latter authors studied axisymmetric convection in large but finite-Γ cylindrical containers with stress-free rather than non-slip horizontal boundaries. Thus, the quantitative applicability of their results to experiments is limited. An interesting feature of these calculations is that although convection begins at R_0, where R_0 is the critical Rayleigh number for the stress-free boundary conditions used, the Nusselt number will increase only slowly until $(R-R_0)/R_0$ exceeds $\approx 2/\Gamma^2$. This feature is tied to the finite amplitude allowed at the centre of the container, and in the limit $(\ln\Gamma)^{-1}\to\infty$, the effect vanishes. We also note that Brown & Stewartson (1978, 1979) consider the effect of sidewall heating which causes an imperfect bifurcation.

Ahlers *et al.* (1981) have used the amplitude-equation formalism (Newell & Whitehead 1969; Segel 1969) and their calculated values of N_1 to interpret heat-transport data for liquid helium obtained using a cylindrical geometry and a fixed aspect ratio, $\Gamma = 4.72$. Experimental results for N_1 for liquid helium in a cylindrical geometry have also been obtained by Pfotenhauer (1984), Pfotenhauer & Donnelly (1985), Pfotenhauer, Lucas & Donnelly (1984), Behringer *et al.* (1982) and Behringer & Ahlers (1977, 1982). These previous measurements vary considerably from one experiment to another. It is not always clear whether these variations are due to differences in experimental conditions, or whether they truly reflect the effect of aspect ratio on the flow.

Additional theoretical work that is useful includes the calculations by Charlson & Sani (1970, 1971) of the critical Rayleigh numbers for convective modes in a cylindrical container. The variable-Γ apparatus provides a unique test of the cubic dependence of R on layer height d, and a test of the inhibiting effect of the sidewalls on the onset of convection.

The remainder of this paper is organized as follows. A detailed description of the apparatus is given in §2. In addition to the variable-Γ apparatus by which most of the data were obtained, we also describe two fixed-aspect-ratio experiments with $\Gamma = 6.22$ and 7.87 made by Behringer *et al.* (1980, 1982). We discuss experimental procedures and the liquid properties which determine the Rayleigh and Prandtl numbers for our experiments in §3. In particular, we discuss the extent to which our experiments satisfy the Oberbeck–Boussinesq approximation. We present our results in §4 where we compare them to theory and previous work. Section 5 contains a summary.

2. Apparatus

2.1. *General arrangement: variable-Γ experiments*

Much of the peripheral apparatus bears an overall similarity to that described by Behringer & Ahlers (1982), and we refer the interested reader to that work. In this

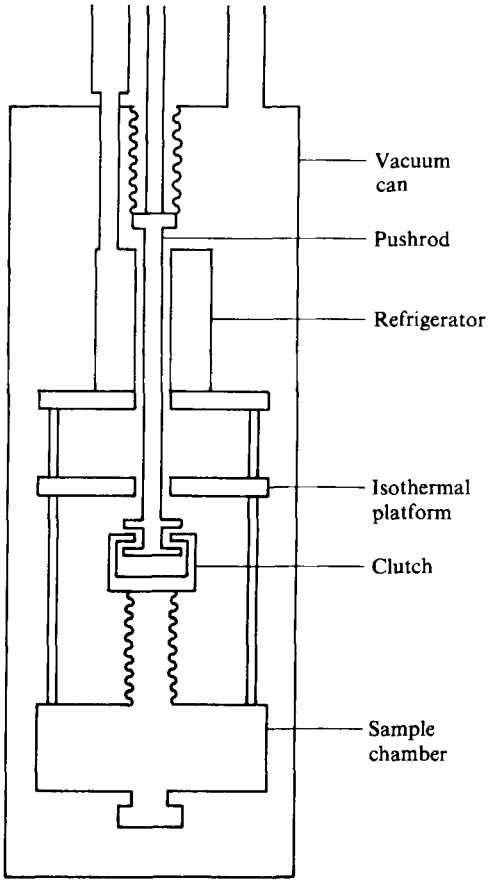

FIGURE 1. Schematic of low-temperature portion of variable-Γ apparatus.

subsection we briefly describe the general features of the experiment, and in the following subsection we focus on the new features that allow us to vary Γ *in situ* with high precision. A third subsection describes pertinent electronics, and the final subsection describes two fixed-aspect-ratio containers.

The low-temperature portion of the experiment consists of a conventional cryostat having a vacuum can immersed in liquid ^{4}He at 4.2 K. The cryostat rests on bellows-sealed antivibration mounts. The apparatus inside the vacuum can is depicted in figure 1. Immediately below the top of the vacuum can is a continuously operating ^{4}He refrigerator after De Long, Symko & Wheatley (1971). The refrigerator is annular in shape in order to allow a pushrod to extend from a bellows seal at the vacuum can to the sample volume. The pushrod also extends up to the top of the cryostat where it is driven by a screw mechanism. The pitch of the screw is sufficiently gentle that we can vary d by steps as small as 1×10^{-2} mm corresponding to changes in Γ of about 1 %. However, these changes can be resolved with much greater precision as discussed later. Below the refrigerator is an isothermal platform (Ahlers 1971) followed by the sample chamber.

2.2. *Sample chamber: variable-Γ experiments*

As shown in figure 2, the sample chamber is modularly constructed of oxygen-free high-conductivity (OFHC) copper, and the pieces are sealed together using indium

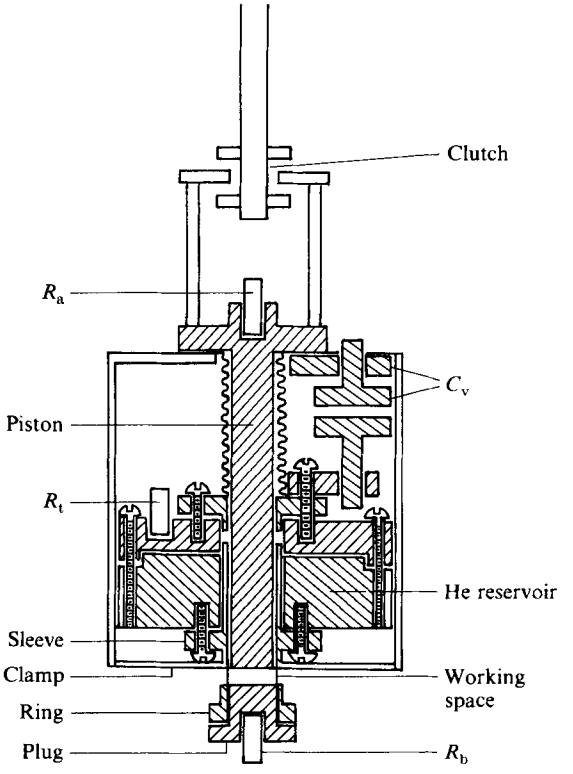

FIGURE 2. Scale drawing of sample chamber used in the variable-Γ experiments.

o-rings. The body contains several hundred 1.5 mm diameter holes which provide for a 12 cm^3 reservoir of liquid ^{4}He at saturated vapour pressure. This technique guarantees rapid thermalization of the liquid and a large thermal 'mass'. The variable-aspect-ratio convection apparatus, which has cylindrical geometry, is an integral part of the sample chamber. Both the upper and lower boundaries of the fluid layer are formed by cylinders made of OFHC copper. The lower boundary consists of an OFHC copper plug which seals one end of a thin (0.012 cm wall) stainless-steel tube. The seal is made by first soldering an OFHC copper ring on the outside of the tube and then by securing the plug to the ring with screws and epoxy (Emerson and Cummings, no. 1266). The ring provides good thermal contact to the walls at the level of the lower liquid boundary. The upper boundary is the face of a moveable OFHC copper piston which slides inside the stainless-steel tube. Thus, in changing the aspect ratio we change the height of the layer at fixed radius. The clearance between tube and piston, as measured at room temperature, is 0.00062 cm on the radius. This tolerance was achieved by soldering the tube into an OFHC copper sleeve, boring out the inner diameter on a well-aligned lathe, and then turning the piston to size. A close tolerance is desirable for two reasons. First, the horizontal surfaces bounding the fluid will only remain parallel if the gap between the piston and the tube is small. Secondly, when the gap is small the possibility of poor thermal contact where the liquid, vertical surfaces, and horizontal surfaces meet will be minimized. In order to provide further thermal contact to the walls, a copper clamp at the top temperature moves with the piston and makes contact with the outside of the wall

at the level of the top plate–fluid interface. The copper sleeve containing the stainless-steel tube is sealed with an indium o-ring into the bottom of the sample chamber. The piston is attached to a bellows which is also sealed to the sample chamber with indium o-rings.

The faces forming the horizontal boundaries of the fluid are polished to a reflecting finish, and then tested for flatness using a monochromatic light source and an optical flat to form an air wedge. The faces are flat to within about 2 μm, compared with a typical value of d of about 1 mm.

The choice of dimensions of the region containing the convecting fluid represented a compromise between a number of competing considerations. Of primary importance was a desire to have aspect ratios stretching from very small to moderately large values. It is useful to have the diameter of the convection region as large as possible in order to minimize the effect of the vertical walls. However, we could not allow the diameter, and hence d, to become so large that the critical temperature differences $\Delta T_c \propto d^{-3}$ became too small. Similarly, if too small values of d were used the fluid would cease to satisfy the Oberbeck–Boussinesq approximation discussed below; also geometric imperfections would be difficult to avoid. A final consideration in determining the diameter of the convection region was the characteristic times anticipated for the flows. There are two relevant timescales: $t_v = d^2/\kappa$, the vertical thermal diffusion time, and $t_h = D^2/4\kappa = \Gamma^2 t_v$, the horizontal thermal diffusion time. If d was made too large, excessively large observation times would be necessary; conversely, if d was made too small, the instrumental time constants could have greatly exceeded t_v.

2.3. *Thermometry and height measuring electronics: variable-Γ experiments*

Temperatures were measured using germanium resistors calibrated against the ^4He vapour-pressure temperature scale, T_{58}, (Dijk *et al.* 1960) and five-lead bridge techniques (Mueller, Ahlers & Pobell 1976). One bridge containing the germanium thermometer R_t was used to regulate the top (cold) temperature (figure 2). A second bridge was used to measure the resistance ratio of thermometer R_b to thermometer R_a, yielding a differential measurement of the temperature difference across the layer. The five-lead differential technique has the advantage of being relatively insensitive to any small changes in self heating or lead resistances. Also, the parasitic heating from the thermometer injected into the bottom of the layer is half as large with a differential configuration as with a direct measurement of the bottom-plate germanium thermometry resistor R_b against a fixed standard resistor attached to the bottom.

The height of convection layer was measured by means of a capacitative technique as depicted in figures 2 and 3. This arrangement requires a fixed capacitor C_f and a variable capacitor C_v which serves as a transducer of the layer height. C_v is a parallel-plate capacitor with one plate attached to the sample chamber and one plate attached to the piston. The spacing between the plates of C_v was adjusted so that the value of C_v was about 8 pF when the height d of the convection region was zero. The second capacitor, C_f, was a 2 pf silver–mica capacitor heat sunk to the sample chamber. Values of C_v were obtained in terms of the ratio $R_h = C_v/(C_v + C_f)$ via a three-lead bridge circuit shown in figure 3. To a first approximation, $(R_h^{-1} - 1) \propto d$. Typically, over the course of a day or two, R_h was stable to $\delta R_h/R_h \approx 10^{-5}$, implying a similar stability in d and Γ. Over many days, the stability was only about a factor of two worse.

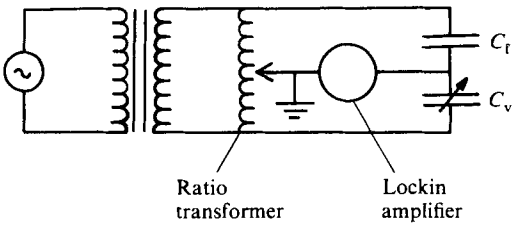

FIGURE 3. Three-lead bridge circuit for measuring C_v. From C_v we determine the height of the layer d. C_f is a fixed capacitor. R_{th} is read directly from the ratio transformer when the lockin amplifier is at null.

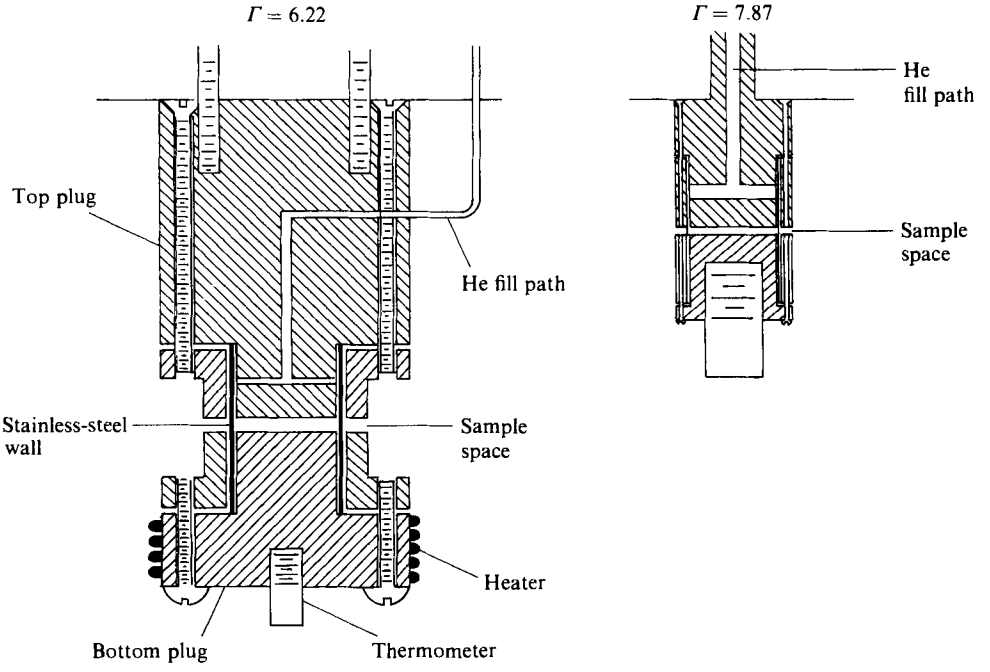

FIGURE 4. Scale drawing of two fixed-aspect-ratio cylindrical containers used by Behringer *et al.* (1982). These containers have aspect ratios of 6.22 and 7.87.

2.4. *Fixed aspect ratios* – $\Gamma = 6.22$ *and* 7.87

Included in this work are results obtained with two fixed-aspect-ratio cylindrical containers having $\Gamma = 6.22$ and 7.87 respectively. Time-dependent flows obtained with these have been presented by Behringer *et al.* (1982). As sketched in figure 4, these containers consist of thin-walled (0.012 cm) stainless-steel tubes sealed at both ends by OFHC copper inserts. These inserts are attached to the tube with epoxy (Emerson and Cummings, 1266) and screws via OFHC copper rings. Dimensions obtained at room temperature are given in table 1. Except for their fixed aspect ratio, these containers are qualitatively similar to the variable-aspect-ratio experiment.

Container	Diameter d (mm)	Height d (mm)
$\Gamma = 6.22$	12.46	1.002
$\Gamma = 7.87$	8.992	0.572
variable-Γ	12.41	2.62 (maximum)

TABLE 1. Dimensions

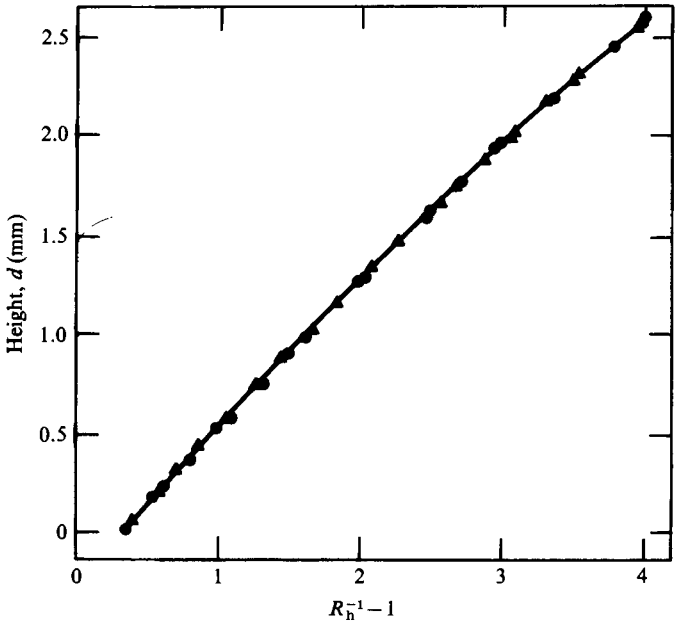

FIGURE 5. Height d versus $R_h^{-1}-1$ direct measurement at room temperature (triangles) and by thermal conductance (circles). The solid curve represents a least-squares fit.

However, they were mounted in a different cryostat which is described by Shaumeyer & Behringer (1986). In this case, differential thermometry was not used. Rather, as in the work of Behringer & Ahlers (1982), the top temperature was held fixed and the bottom temperature was measured via a germanium resistance thermometer paired with a fixed resistor in a five-lead a.c. bridge. Thermometers for the top and bottom were calibrated against both the T_{58} ^{4}He temperature scale (Dijk *et al.* 1960) and the T_{62} ^{3}He temperature scale (Sydoriak, Sherman & Roberts 1964).

3. Procedures and fluid parameters

3.1. *Procedures*

Before cooling to liquid-helium temperatures, the height d of the variable-Γ apparatus was calibrated as a function of C_v using a micrometer reading to the nearest 0.00025 cm. Values of d were deduced by measuring the displacement of the piston relative to its fully closed position. The condition $d = 0$ provided a reproducible reference which was independent of the small changes associated with cooling from room temperatures to liquid-helium temperatures. Figure 5 shows d versus $(R_h^{-1}-1)$

from a typical calibration. Except for the fringing effects at large d, the result is a nearly straight line as expected. This calibration method has the disadvantage of being a room-temperature calibration. Accordingly, we also determined d as a function of R_h by the thermal conductance $Q/\Delta T$ of the fluid-filled container; here Q is the heat flux traversing the layer. Under steady conditions below the onset of convection $Q/\Delta T \propto d^{-1}$ independent of ΔT. In order to obtain the proportionality constant between $Q/\Delta T$ and d, we required that the measured fluid conductivity agree with existing measurements for the thermal conductivity of ^{4}He (Kerrisk & Keller 1969; Ahlers, Hohenberg & Kornblit 1982). A comparison between the two calibration methods in figure 5 shows an agreement that is within a few percent over the full range of d. Accordingly, uncertainty in Γ is of the same size, although the precision with which successive values of Γ can be determined is much higher.

Before liquid was condensed into the sample chamber, the vertical wall (empty) conductivity was measured as a function of temperature. For the variable-Γ apparatus the wall conductivity was obtained at a number of different aspect ratios. After the liquid was condensed into the sample chamber, data taking was initiated by obtaining a value of the differential thermometer (bottom thermometer for fixed-aspect-ratio containers) without an applied heat current. Then, a heat current, measured by a four-lead potentiometric method with a precision of 0.03 %, was supplied through a non-inductive wire-wound resistance ($\approx 5\,\mathrm{k\Omega}$) glued to the bottom of the convective cell with GE 7031 varnish. This heat current was typically set initially to less than the critical value needed to generate convection. Following an equilibration time, the heat current was increased in small steps with intervening times of $15t_v$ to $20t_v$. From time to time the heater current was turned off to check for drifts in the thermometers.

3.2. *Fluid properties*

Barenghi, Lucas & Donnelly (1981) have made a very useful tabulation of the fluid properties of liquid ^{4}He at saturated vapour pressure, and they have presented their results in the form of spline fits. From these data, we have calculated the Prandtl number for the various temperatures used in our experiments. Most of our data were obtained for $0.50 \leqslant Pr \leqslant 0.75$, although some data were obtained for Pr as large as 0.9.

A particular relevant question concerns the Oberbeck–Boussinesq approximation (Oberbeck 1879; Boussinesq 1903). Although we could initiate convection in the variable-Γ apparatus for aspect ratios up to $\Gamma = 25$, we have limited our studies to $\Gamma \lesssim 16$ to guarantee clearly Boussinesq flow. A quantitative measure, Q_{OB}, of the departure from this approximation has been given by Busse (1967) (see also Walden & Ahlers 1981). We have calculated values of Q_{OB} at R_c for cases relevant to our experiments (see table 2). In these calculations we have again used the thermo-hydrodynamic data tabulated by Barenghi *et al.* (1981) and assumed that R_c can be approximated by 1707.8. We find that $|Q_{OB}| \lesssim 0.03$ for most of our measurements; the largest value of $|Q_{OB}|$ is 0.26.

4. Results

4.1. *Critical Rayleigh numbers*

The critical Rayleigh number is determined from (2) once the critical value ΔT_c of ΔT is determined. Values of ΔT_c were determined by fitting the Nusselt number $N(\Delta T)$ to a polynomial and then determining the intersection of the polynomial with

the line $N = 1$. Typical examples of N are given in figures 6–9 and discussed in the following section. Owing to the presence of some small amount of rounding in the heat-transport curves, a given fit was made with a lower limit on the allowed ΔT's that was slightly greater than the estimated ΔT_c. Some of the rounding may be due to the effect of the sidewalls as discussed in §1; i.e. N may increase very slowly with R just above R_c even though the bifurcation is sharp. However, it is difficult to determine whether this is the case or whether the rounding is caused by very small flaws in the apparatus which lead to an imperfect bifurcation. Since, experimentally, the amount of rounding in N, expressed as a function of R/R_c, depends very little on Γ, we may have systematically overestimated ΔT_c by a small but in percentage terms nearly uniform amount. The largest ΔT included in a fit was limited for larger aspect ratios by the presence of a transition to a time-dependent flow state occurring at a Rayleigh number which we define to be R_1. Typically $R_1/R_c \approx 1.1$ when Γ is large. Values of R_1/R_c and a discussion of flows near R_1 have been given by Behringer *et al.* (1983) and by Gao & Behringer (1984); a more extensive discussion, will be given in Part 2 of this work.

Fits of $N(\Delta T)$ were made with linear and quadratic polynomials in ΔT, and the resulting values of ΔT_c were found to be relatively insensitive to the degree of polynomial. The quality of the fit as measured by the standard deviation was not usually improved significantly by the presence of a quadratic term as long as values of $\Delta T/\Delta T_c$ were restricted from the curved region near R_c and the region well above R_c where the Nusselt curve develops significant downward curvature.

The largest errors in determining R_c come from uncertainty in the fluid parameters. Of these, the greatest uncertainty probably occurs for the shear viscosity η and hence ν. The combined uncertainty in R_c from κ, ν and α_p is probably at least 20%, a relative uncertainty considerably larger than those in d or ΔT_c. Using a typical aspect ratio, $\Gamma = 5.330$ we obtain from the measured ΔT_c and fluid parameters a value of $R_c = 1510 \pm 300$ which is in agreement with the expected value. Accordingly, we have chosen to present results for R_c that have been normalized at a relatively large aspect ratio to the predicted value 1707.8 for an infinite layer; these normalized values are shown in figure 10. By normalizing our data we also largely removed ambiguities as to whether the onset of convection occurs at the beginning of the rounded region or at a slightly higher Rayleigh number. The data agree within the scatter of a few percent with the squares which give theoretical predictions for R_c by Charlson & Sani (1970) applicable for $\Gamma \lesssim 8$. These predictions pertain to the axisymmetric modes in a cylindrical container with insulating sidewalls. Critical Rayleigh numbers for non-axisymmetric modes have also been calculated by Charlson & Sani (1971), but the difference in critical Rayleigh numbers between the various types of modes is usually too small to be observed experimentally unless the aspect ratio is very small. We also show in figure 10 predictions by Ahlers *et al.* (1981) for parallel rolls in a circular container (dash-dot line) and an axisymmetric flow pattern with a central node (dashed line). In these cases as well, the data for R_c cannot distinguish the pattern, although, on average, the data tend to fall somewhat lower than the predictions for axisymmetric flow with a vanishing amplitude at the centre. Likewise, the small ripples in the values $R_c(\Gamma)$ predicted by Charlson & Sani (1970) and associated with changes in the number of convection rolls cannot be detected in the present experiments. The data of figure 10 do provide a particularly strong test of the rapid dependence of R on d, since in these data d^3 varies by a factor of about 300.

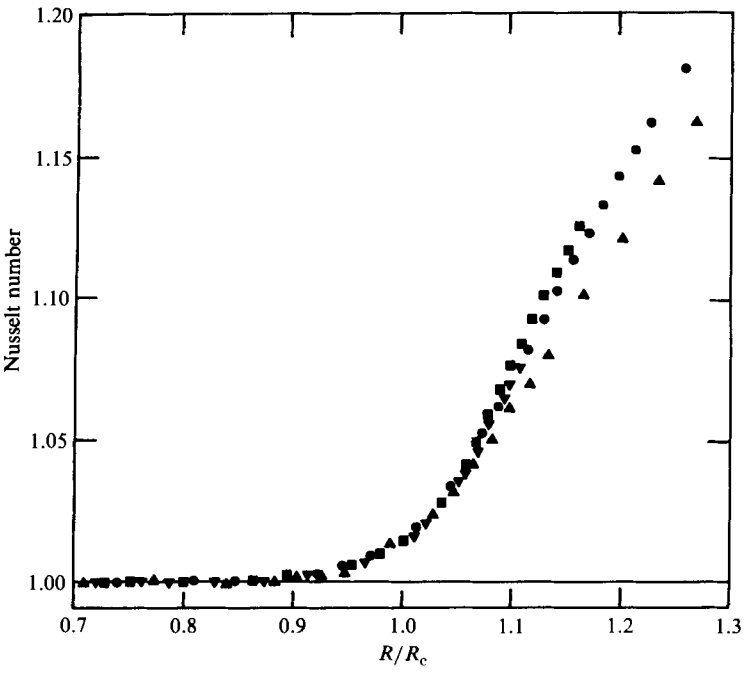

FIGURE 6. The Nusselt number N versus R/R_c for four cases which sample the range of variable aspect ratios. ▲, $\Gamma = 2.387$; ●, 7.604; ■, 12.093; ▼, 15.770. Except for $\Gamma = 2.387$, the data shown span the complete range of time-independent convective states.

Γ	Pr	N_1	$-Q_{OB}$	Γ	Pr	N_1	$-Q_{OB}$
2.387	0.77	0.609	0.003	6.752	0.56	0.656	0.013
2.604	0.75	0.552	0.002	6.858	0.56	0.603	0.014
2.811	0.75	0.524	0.003	7.086	0.56	0.680	0.015
2.941	0.75	0.556	0.003	7.322	0.56	0.714	0.016
3.157	0.75	0.386	0.004	7.604	0.56	0.735	0.020
3.568	0.75	0.609	0.006	7.848	0.56	0.681	0.021
3.746	0.75	0.602	0.007	8.130	0.56	0.646	0.022
3.946	0.65	0.675	0.004	8.224	0.56	0.707	0.023
4.550	0.71	0.518	0.008	8.390	0.56	0.722	0.025
4.771	0.71	0.656	0.009	8.650	0.56	0.746	0.027
4.829	0.59	0.672	0.005	8.909	0.56	0.709	0.030
5.049	0.71	0.646	0.011	8.994	0.50	0.648	0.052
5.286	0.71	0.621	0.012	9.138	0.56	0.665	0.032
5.311	0.71	0.626	0.012	9.395	0.56	0.704	0.035
5.330	0.57	0.526	0.006	9.411	0.56	0.690	0.035
5.815	0.71	0.613	0.016	10.814	0.50	0.687	0.090
6.070	0.71	0.683	0.019	11.735	0.56	0.770	0.068
6.070	0.56	0.669	0.013	12.093	0.56	0.773	0.074
6.070	0.59	0.668	0.012	12.319	0.56	0.780	0.080
6.244	0.56	0.704	0.010	12.591	0.56	0.750	0.084
6.300	0.71	0.691	0.020	12.610	0.50	0.710	0.14
6.485	0.56	0.715	0.010	12.823	0.56	0.787	0.088
6.573	0.71	0.652	0.024	15.770	0.53	0.733	0.26

TABLE 2. Values of the initial slope N_1

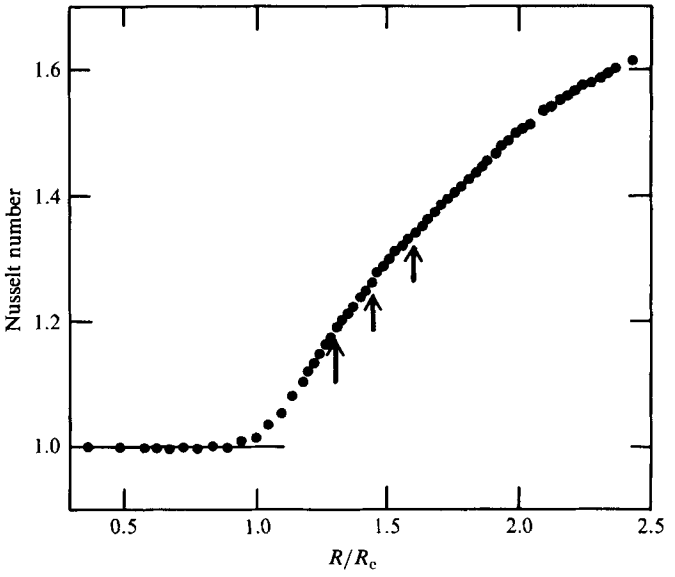

FIGURE 7. Nusselt number N versus R/R_c for $\Gamma = 2.387$. The arrows indicate transitions in the flow pattern. At this point the Nusselt number is discontinuous.

4.2. *Heat transport*

Measurements of N just above R probe the weakly nonlinear flow in that region. Typical results for $N(R)$ are given in figures 6–9, and in a compact form as $N_1(\Gamma)$ in figure 11 and table 2. Several features of figure 11 are noteworthy. In particular, for not too small aspect ratios, $\Gamma \gtrsim 6$, the values of N_1 obtained in the present experiments fall quite close to the large-Γ value 0.72 predicted by Ahlers *et al.* (1981) for straight parallel rolls in a cylindrical container. Although there is an overall increase in N_1 with aspect ratio, for $\Gamma \gtrsim 6$, the increase is quite slow. Ahlers *et al.* (1981) predict such a slow variation with Γ for the case of cylindrically symmetric flow with a central node. For instance, from figure 1 inset of Ahlers *et al.* (1981), we obtain the thin solid curve in figure 11. This curve, which attempts to give the general sense of their results, shows $(N-1)/\epsilon$ from figure 1 of Ahlers *et al.* assuming typical ϵ-values (0.3 to 0.1 as Γ changes from 2.4 to 16) for the fits in the present experiments. However, for the case of parallel rolls in a cylindrical container comparable calculations do not yet exist.

The data show oscillatory variations, particularly at low aspect ratio, emphasized by the solid curves, which reflect the number of convection rolls present. The vertical bars, indicating the period of the oscillations in $N_1(\Gamma)$, are obtained independently from oscillations in R_1 as a function of Γ as given by Behringer *et al.* (1983) and Gao & Behringer (1984). The data for R_1 are particularly sensitive to the number of convection rolls and provide a clear indication of changes in the flow pattern with changing Γ. Although current theory for finite Γ does not, to our knowledge, describe these variations of N_1 with the number of convection rolls, it is reasonable to expect them to occur. It is possible to make a rough comparison with calculations by Clever & Busse (1974) pertaining to a horizontally infinite layer, which give $N(R)$ for several wavevectors α and for several Prandtl numbers. From their calculations at $Pr = 0.71$, we estimate that the fractional change of N_1 with α is $N_1^{-1}\, \mathrm{d}N_1/\mathrm{d}\alpha \approx 0.6$.

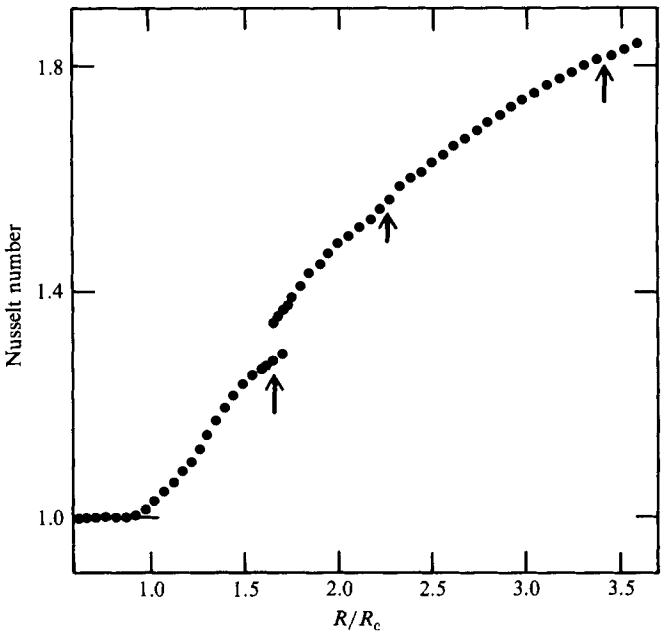

FIGURE 8. Nusselt number N versus R/R_c for $\Gamma = 3.157$. As in figure 7, the arrows indicate changes in the convective roll pattern.

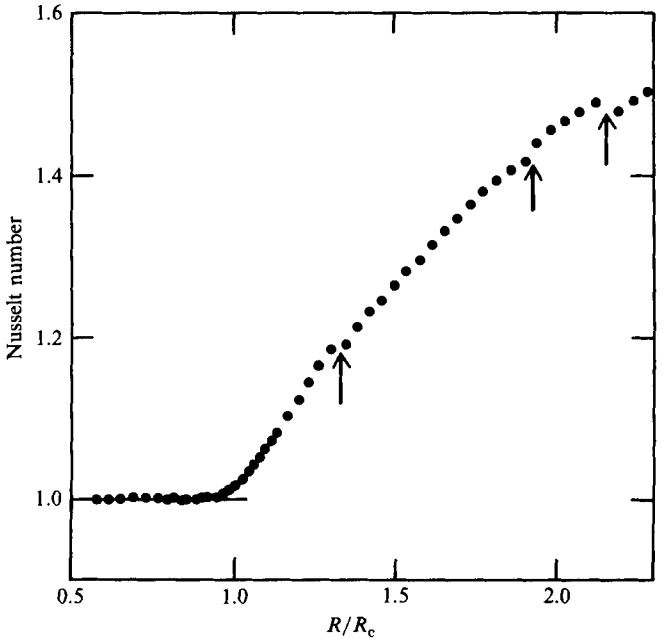

FIGURE 9. Nusselt number N versus R/R_c for $\Gamma = 3.568$. As in the two preceding figures, the arrows indicate changes in the convective flow patterns.

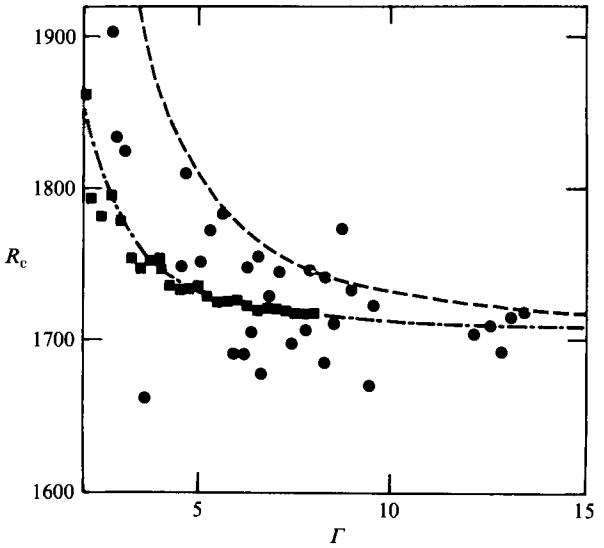

FIGURE 10. Solid circles give values of R_c versus Γ. The values of R_c have been normalized at large Γ to the value $R_c = 1708$. The squares represent the calculations of Charlson & Sani (1970) for insulating sidewalls. Other curves give the values of R_c calculated by Ahlers *et al.* (1981) for parallel rolls (— · — · — · —), and axisymmetric rolls with a central node (— — — —).

We obtain an estimate of α by assuming, as in Gao & Behringer (1984), that $\alpha \approx n(\frac{1}{2}\pi\Gamma)$ where n is an integer which gives the number of rolls, if the rolls are nearly parallel, or twice the number of toroidal rolls, if the pattern is axisymmetric. A reasonable set of wavevectors is obtained if we assume $n = 6$ for the region between our lowest aspect ratio, $\Gamma = 2.4$, and the left-most dashed line of figure 11, and if we assume that n changes by 2 each time a vertical dashed line is crossed. On crossing a vertical dashed line, the change in wavevector is then approximated as

$$\Delta\alpha \approx \frac{\pi}{\Gamma}; \tag{11}$$

the corresponding change in N_1 is then approximated by

$$\Delta N_1 \approx \frac{0.6\pi N_1}{\Gamma}. \tag{12}$$

An inspection of figure 11 shows that this procedure overestimates the experimentally observed changes in N_1 by a factor between 2 and 4. Given the *ad hoc* nature of the assumptions used in the comparison, this level of agreement is probably satisfactory.

It is interesting to compare our data with previous results reported by Behringer & Ahlers (1982) for aspect ratios 2.08, 4.72 and 57, results reported by Pfotenhauer (1984), Pfotenhauer & Donnelly (1985), and Pfotenhauer *et al.* (1984), for aspect ratios 7.81 and 4.93, and results reported by Behringer *et al.* (1982) for aspect ratios 6.22 and 7.87. All these results pertain to liquid helium in cylindrical containers. N_1 values for these experiments are displayed in figure 12; the results of this work are represented by the solid curves and some solid circles in order to avoid confusion. In general there is only approximate agreement among the various sets of data, with some exceptions. In particular the results by Behringer *et al.* (1982) for $\Gamma = 7.87$ are

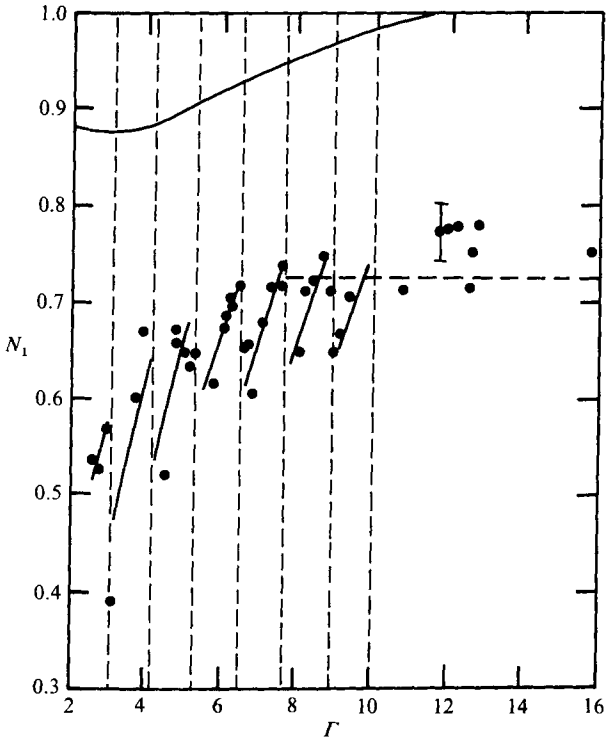

FIGURE 11. Experimental values of N_1, the initial slope of the Nusselt–Rayleigh curve versus aspect ratio Γ. The heavy horizontal dashed line is the prediction, in the large-Γ limit, by Ahlers *et al.* (1981) for parallel rolls in a cylindrical container. Solid heavy lines indicate the oscillations in N_1 which are superposed on an overall increase of N_1 with aspect ratio when Γ is small. The vertical dashed lines correspond to changes in the number of convection rolls, as inferred from data by Behringer *et al.* (1983), and Gao & Behringer (1984). Also shown as the thin solid line is an estimate, based on the multimode analysis of Ahlers *et al.* (1981), for N_1 when the flow pattern is axisymmetric with a central node.

significantly lower – by an amount exceeding experimental error – than others for nearby Γ-values. We speculate that the flows in this container were qualitatively different from those in other experiments with comparable aspect ratios. Different flow patterns in similar geometries may be generated by differences in the thermal properties of the sidewalls and the way in which a steady state is reached. To our knowledge, however, there are no calculations that address which pattern will form in a cylinder as the sidewall thermal conditions change. The result of Ahlers *et al.* (1981) and of Behringer & Ahlers (1982) for $\Gamma = 4.72$, namely $N_1 = 0.83$ for $Pr = 0.78$, falls higher than the present data. However, these experiments were complicated by the presence of a state towards which the flow seemed to evolve initially, but which was not stable relative to the final pattern. An estimated slope for the 'metastable' state, $N_1 = 0.56$, falls near the range found for the variable-Γ experiments. In the present work no metastable states were ever observed. However, the small steps in R/R_c and the long waiting times of $\approx 20t_v$ would not have revealed transient states, such as those reported by Ahlers *et al.* (1981) and by Behringer & Ahlers (1982), which decayed in times less than or order of $20t_v$. The results of Pfotenhauer (1984) and Pfotenhauer *et al.* (1984) show significant variations in N_1 which are not systematically

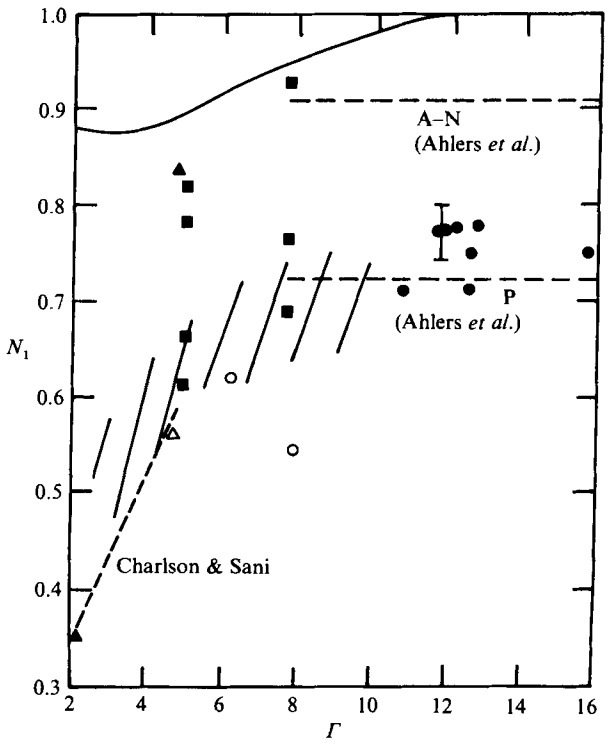

FIGURE 12. Comparison of N_1 versus Γ from previous data by Pfotenhauer *et al.* (1984) (■), Behringer & Ahlers (1982) (△ (obtained from data for a metastable state), ▲). Behringer *et al.* (1982) (○), and present data (———, ●). Horizontal dashed lines show, in the large-Γ limit, theoretical predictions by Ahlers *et al.* (1981) for single-mode axisymmetric flow with a central node (A–N), and parallel rolls (P). The upper thin solid line is derived from the multimode calculation of Ahlers *et al.* (1981) for axisymmetric flow with a central node. The sloping dashed line passes through two values of N_1 calculated by Charlson & Sani (1975) for axisymmetric flow in a container with insulating sidewalls ($Pr = 1$).

related to variations in Pr or Γ. For $\Gamma = 7.81$, for instance, the values of N_1 seem to fall either near $N_1 \approx 0.91$ or 0.72. As noted by these authors, these results cannot be understood in terms of the predicted slope of any one flow state, nor can Prandtl-number effects, which are expected to be negligible over $0.5 \lesssim Pr \lesssim 1.0$, (Schlüter *et al.* 1965; Ahlers *et al.* 1981) reasonably account for these observations. That N_1 does vary only weakly with Pr is demonstrated in figure 13 where we show fractional variations of $N_1(Pr)$ for $\Gamma = 12.523$; the solid line represents the relative variations in N_1 expected from the infinite-aspect-ratio calculations of Schlüter *et al.* (1965). Thus, Pfotenhauer *et al.* suggest that more than one pattern routinely formed in their experiments.

Also indicated as dashed lines in figure 12 are the theoretical predictions of N_1 by Ahlers *et al.* (1981) for flow patterns with parallel rolls (P), and the single-mode approximation for axisymmetric rolls with a central node (A−N). Although results for the slope for an axisymmetric flow with a finite centre amplitude exist (Brown & Stewartson 1978, 1979; Ahlers *et al.* 1981), they pertain to stress-free horizontal boundaries which do not apply to these experiments; accordingly, these results are not shown in figure 12. We also show by the upper thin solid line an estimate of the

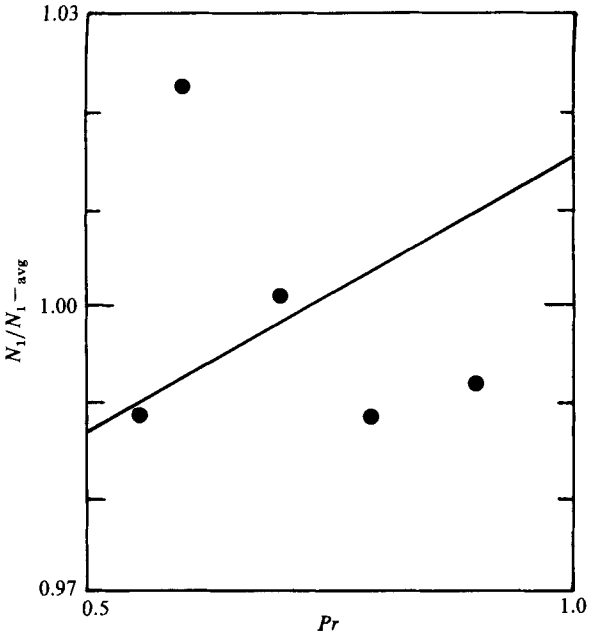

FIGURE 13. Relative variations in the initial slope N_1 versus Prandtl number Pr for the fixed aspect ratio 12.932. The solid line indicates the fractional variation of N_1 expected on the basis of theory (Ahlers *et al.* 1981; Schlüter *et al.* 1965).

prediction for an axisymmetric pattern with a central node based on the multimode analysis of Ahlers *et al.* (1981), as discussed above. The slanted dashed line was drawn through the insulating-sidewall values of N_1 predicted by Charlson & Sani (1975) for $\Gamma = 1.00$ and 2.25; this curve forms an approximate lower bound to the experimental data in the applicable region.

4.3. *Experimental error*

In addition to the direct measurement errors, which are typically smaller than 0.1 % in N and therefore affect N_1 very little there is a possible systematic error associated with removing the contribution of the vertical walls from the measured heat flux. Errors in determining the wall contribution lead to an error δN_1 in N_1 of

$$\frac{\delta N_1}{N_1} = \frac{\lambda_w}{\lambda_L}\frac{\delta\lambda_w}{\lambda_w}, \tag{13}$$

where $\delta\lambda_w/\lambda_w$ is the fractional uncertainty in the vertical wall conductance λ_w, and λ_L is the conductance of the liquid. Typically, $\lambda_w/\lambda_L \approx 0.25$. The precision with which λ_w is obtained is better than 0.1 %, although it is conceivable that systematic errors are higher. These systematic errors can occur if the vertical walls are not completely attached thermally at the top and bottom boundaries. In this case, the wall conductance that is measured in the absence of liquid is lower than that with liquid. Thus, subtracting an empty conductivity does not correctly account for the wall contribution. In addition, walls with finite, non-zero thermal conductivity can support horizontal heat flow which is also not rigorously accounted for by subtracting an empty conductivity for vertical heat flow. We believe such effects to be small but

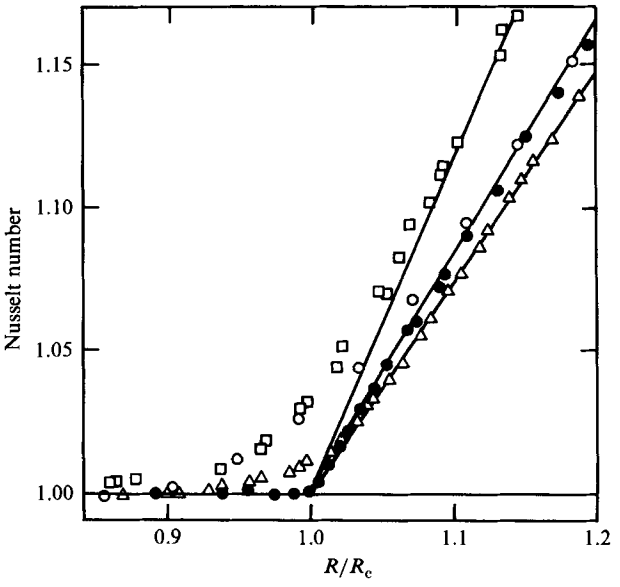

FIGURE 14. Nusselt number N versus R/R_c showing the rounded region near the onset of convection. The symbols indicate data for $\Gamma = 57$ (□) and $\Gamma = 4.72$ (●) by Behringer & Ahlers (1982), data for $\Gamma = 5.27$ by Ahlers (1975) (○), and data for $\Gamma = 8.390$ by the present authors (△).

still present in recent helium measurements. It seems possible that errors in the wall conductivity could create systematic uncertainties in N_1 of up to a few percent, but not much more.

4.4. *Rounding near onset*

We turn now to the small amount of rounding observed near R_c. In figure 14, we compare the amount of rounding in the present data with previous measurements. Our results show more rounding than those of Behringer & Ahlers (1982) for $\Gamma = 4.72$ but less than their results for $\Gamma = 57$ or the data of Ahlers (1975) for $\Gamma = 5.27$. Surprisingly, we find little variation in the amount of rounding as we vary Γ. This is shown in figure 6 which provides a comparison of data near onset for aspect ratios spanning the range of our data.

Rounding observed near R_c in the heat transport is usually attributed either to imperfections in the cell geometry (Kelly & Pal 1978) or to imperfect thermal boundaries such as poorly attached sidewalls (Daniels 1977; Hall & Walton 1977; Brown & Stewartson 1978, 1979). For our experimental arrangement, both geometrical defects and sidewall heating are very small, but the difference in the two effects should depend on aspect ratio. In particular if the rounding is caused by spatial inhomogeneities, such as a variation in height throughout the layer by $\pm\delta d$, we would expect that the rounding would increase with Γ in the present apparatus. This follows because d will decrease with increasing Γ, whereas δd presumably remains fixed. On the other hand, if the rounding is attributable to sidewall heating effects, it should depend less sensitively on aspect ratio. As discussed previously, the finite size of the container may also lead to a weak variation in $N(R)$ near onset which, in an experiment, would be difficult to separate from rounding due to imperfections. For axisymmetric flow with a finite centre amplitude, Brown & Stewartson (1979)

find that such an effect will occur over a reduced Rayleigh-number range of $\approx 2/\Gamma^2$. This prediction is not consistent with our observations. Given our ignorance of the details of any imperfections, our uncertainty of the flow patterns, and the lack of theory describing rounding for non-slip boundaries, we have not attempted a detailed analysis of the experimental rounding.

4.5. *Comparison with room-temperature experiments*

As a final comment, we note that recent flow visualization in convecting cylindrical layers of water ($Pr \approx 4$) show time-dependent behaviour very near R_c. The time dependence consists of changes in the convection pattern and occurs for $R_c \lesssim R \lesssim 1.3R_c$. In these measurements by Heutmaker, Fraenkel and Gollub (1985) and by Ahlers *et al.* (1985) no variations in $N(R)$ were detectable to a level of 0.1 %. In our measurements, which have a best-case resolution of 0.005 %, no time dependence in N was seen for $R_c \leqslant R \leqslant R_1$. The time dependence beginning at R_1 consists of steady periodic oscillations. We note that Pocheau *et al.* (1985) have recently reported flow-visualization measurements on room-temperature argon gas in a cylindrical container with a Prandtl number $Pr = 0.69$. They find steady flow patterns of approximately parallel rolls up to a value of R_1 comparable with values found in liquid-helium experiments of similar Prandtl number. Just above R_1 they report periodic time dependence. Although J. P. Gollub & M. S. Heutmaker (1984, private communication) report periodic time dependence at higher R in water, a quantitative comparison with the lower-Pr experiments is not yet possible. Indeed, the relation between the low-Pr liquid-helium and argon-gas measurements and those at higher Pr made with room-temperature fluids needs clarification.

5. Summary

We have first provided details of an apparatus that allows us to make high-precision measurements of the Nusselt number N as a function of the Rayleigh number R. We can adjust the aspect ratio of the apparatus in the range $2.4 \leqslant \Gamma \leqslant 25$, although we have limited our results to $\Gamma \lesssim 16$ in order to clearly avoid non-Boussinesq effects.

The primary results presented here are values of the slope $N_1 = R_c\,\mathrm{d}N/\mathrm{d}R$ evaluated in the weakly nonlinear regime just above R_c. Our data show in a consistent way how the Nusselt number responds to variations in the aspect ratio. Values of N_1 with $6 \lesssim \Gamma \lesssim 16$ are in agreement with the variational prediction by Ahlers *et al.* (1981) who give $N_1 = 0.72$ for straight parallel rolls confined in a cylindrical geometry. We suggest that in our larger-aspect-ratio range, the convection pattern is usually characterized by approximately straight rolls. In support of this suggestion we note the agreement between the data and the parallel-roll prediction, and the observation from room-temperature experiments that non-axisymmetric patterns usually form when R is increased gradually, as in our experiments. For $\Gamma \lesssim 6$ the vertical walls cause a substantial reduction in N_1. For the small-aspect-ratio range of our experiments, there is less theoretical information regarding the flow pattern, which may vary significantly as Γ changes by ≈ 1. An interpolation between predictions of N_1 by Charlson & Sani (1975) for axisymmetric flows in small-aspect-ratio containers falls just below our data, and indeed, these interpolated results overlap our data for several of the smaller aspect ratios.

Some rounding is visible in our data. Because the amount of rounding is nearly independent of Γ, we attribute it to the small sidewall heating effects and possibly the effect of finite aspect ratio.

Results for N_1 obtained by other experimenters include those by Pfotenhauer (1984), Pfotenhauer *et al.* (1984), Behringer *et al.* (1982), Behringer and Ahlers (1982) and Ahlers (1975). Some of these agree with our results. However, in some cases there is considerable disagreement and it seems unlikely that these experiments and our own at the same aspect ratio share the same flow pattern.

In this work we also present a unique test of the cubic dependence of the critical Rayleigh number on d. Values of R_c are in good agreement with expectations.

Notably, no time dependence was observed for $R_c \leqslant R < R_1$, where R_1 is the Rayleigh number for the onset of time dependence. As discussed by Behringer *et al.* (1983) and Gao & Behringer (1984), $R_1 \gtrsim 1.1\ R_c$, with R_1 as low as $1.1R_c$ only for the largest aspect ratios. For $R \gtrsim R_1$, periodic time dependence was seen. These results are similar to recent experiments in argon ($Pr = 0.69$) by Pocheau *et al.* (1985) where straight parallel rolls were seen. Recently, however, Ahlers *et al.* (1985) and Heutmaker *et al.* (1985) have reported non-periodic time dependence very near R_c. These experiments were carried out in moderate-aspect-ratio cylindrical containers using water ($Pr \approx 4$) as the fluid. The time dependence consisted of a continual change in the flow pattern. An interesting question is whether similar time dependence exists in the helium experiments but is not detectable by heat flux measurements. There is no clearly established connection between the low-Prandtl-number helium measurements and those made on room-temperature fluids having larger Prandtl numbers.

This work was supported by the National Science Foundation under Low Temperature Physics Grant No. DMR-8314673. One of us (R.P.B.) acknowledges support by the Alfred P. Sloan Foundation.

REFERENCES

AHLERS, G. 1971 Heat capacity near the superfluid transition in ^{4}He at saturated vapor pressure. *Phys. Rev.* A **3**, 696–716.

AHLERS, G. 1974 Low temperature studies of the Rayleigh–Bénard instability and turbulence. *Phys. Rev. Lett.* **33**, 1185–1188.

AHLERS, G. 1975 The Rayleigh–Bénard instability at helium temperatures. In *Fluctuations, Instabilities and Phase Transitions* (ed. T. Riste), pp. 181–193. Plenum.

AHLERS, G. 1980 Onset of convection and turbulence in a cylindrical container. In *Systems far from Equilibrium* (ed. L. Garrido), pp. 143–161. Springer.

AHLERS, G. & BEHRINGER, R. P. 1978*a* The Rayleigh–Bénard instability and the evolution of turbulence. *Prog. Theor. Phys. Suppl.* **64**, 186–201.

AHLERS, G. & BEHRINGER, R. P. 1978*b* Evolution of turbulence from the Rayleigh–Bénard instability. *Phys. Rev. Lett.* **40**, 712–716.

AHLERS, G., CANNELL, D. S. & STEINBERG, V. 1985 Time dependence of flow patterns near the convective threshold in a cylindrical container. *Phys. Rev. Lett.* **54**, 1373–1376.

AHLERS, G., CROSS, M. C., HOHENBERG, P. C. & SAFRAN, S. 1981 The amplitude equation near the convective threshold: applications to time-dependent heating experiments. *J. Fluid Mech.* **110**, 297–334.

AHLERS, G., HOHENBERG, P. C. & KORNBLIT, A. 1982 Nonlinear renormalization-group analysis of the thermal conductivity of ^{4}He for $T \geqslant T_\lambda$. *Phys. Rev.* B **25**, 3136–3166.

AHLERS, G. & WALDEN, R. W. 1980 Turbulence near onset of convection. *Phys. Rev. Lett.* **44**, 445–448.

BARENGHI, C. F., LUCAS, P. G. & DONNELLY, R. J. 1981 Cubic spline fits to thermodynamic and transport parameters of liquid ^{4}He above the λ transition. *J. Low Temp. Phys.* **44**, 491–503.

BEHRINGER, R. P. 1985 Rayleigh–Bénard convection and turbulence in liquid helium. *Rev. Mod. Phys.* **57**, 657–688.

BEHRINGER, R. P., AGOSTA, C., JAN, J. S. & SHAUMEYER, J. N. 1980 Time dependent Rayleigh–Bénard convection and instrumental attenuation, *Phys. Lett.* **80A**, 273–276.

BEHRINGER, R. P. & AHLERS, G. 1977 Heat transport and critical slowing down near the Rayleigh–Bénard instability in cylindrical containers. *Phys. Lett.* **62A**, 329–331.

BEHRINGER, R. P. & AHLERS, G. 1982 Heat transport and temporal evolution of fluid flow near the Rayleigh–Bénard instability in cylindrical containers. *J. Fluid Mech.* **125**, 219–258.

BEHRINGER, R. P., GAO, H. & SHAUMEYER, J. N. 1983 Time-dependence in Rayleigh–Bénard convection with a variable cylindrical geometry. *Phys. Rev. Lett.* **50**, 1199–1202.

BEHRINGER, R. P., SHAUMEYER, J. N., JAN, J. S., CLARK, C. A. & AGOSTA, C. 1982 Turbulent onset in moderately large aspect ratios. *Phys. Rev.* A**26**, 3723–3726.

BOUSSINESQ, J. 1903 *Théorie Analytique de la Chaleur*, vol. 2. Gauthier-Villas.

BROWN, S. N. & STEWARTSON, K. 1978 On finite amplitude Bénard convection in a cylindrical container. *Proc. R. Soc. Lond.* A**360**, 455–469.

BROWN, S. N. & STEWARTSON, K. 1979 On the finite amplitude Bénard convection in a cylindrical container. *SIAM J. Appl. Maths* **36**, 573–586.

BUSSE, F. H. 1967 The stability of finite amplitude cellular convection and its relation to an extremum principle. *J. Fluid Mech.* **13**, 625–649.

CHARLSON, G. S. & SANI, R. L. 1970 Thermoconvective instability in a bounded cylindrical fluid layer. *Intl. J. Heat Mass Transfer* **13**, 1479–1496.

CHARLSON, G. S. & SANI, R. L. 1971 On thermoconvective instability in a bounded cylindrical fluid layer. *Intl. J. Heat Mass Transfer* **14**, 2157–2160.

CHARLSON, G. S. & SANI, R. L. 1975 Finite amplitude axisymmetric thermoconvective flows in a bounded cylindrical layer of fluid. *J. Fluid Mech.* **71**, 209–229.

CLEVER, R. M. & BUSSE, F. H. 1974 Transition to time-dependent convection. *J. Fluid Mech.* **65**, 625–645.

CROQUETTE, V., MORY, M. & SCHOSSELER, F. 1983 Rayleigh–Bénard convective structures in a cylindrical container. *J. Phys. Paris* **44**, 293–301.

CROSS, M. C. 1982 Ingredients of a theory of convective textures close to onset. *Phys. Rev.* A**25**, 1065–1076.

DANIELS, P. G. 1977 The effect of distant sidewalls on the transition to finite amplitude Bénard convection. *Proc. R. Soc. Lond.* A**358**, 173–197.

DE LONG, L. E., SYMKO, O. G. & WHEATLEY, J. G. 1971 Continuously operating ^{4}He evaporation refrigerator. *Rev. Sci. Instrum.* **42**, 147–150.

DIJK, H. VAN, DURIEUX, M., CLEMENT, J. R. & LOGAN, J. K. 1960 The 1958 ^{4}He Scale of Temperatures. *Nat. Bur. Stand. Monograph no.* 10.

GAO, H. & BEHRINGER, R. P. 1984 Onset of convective time-dependence in cylindrical containers. *Phys. Rev.* **30**, 2837–2839.

HALL, P. & WALTON, I. C. 1977 The smooth transition to a convective regime in a two-dimensional box. *Proc. R. Soc. Lond.* A**358**, 199–221.

HEUTMAKER, M. S., FRAENKEL, P. N. & GOLLUB, J. P. 1985 Convection patterns: time evolution of the wave-vector field. *Phys. Rev. Lett.* **54**, 1369–1372.

HOARD, C. Q., ROBERTSON, C. R. & ACRIVOS, A. 1970 Experiments on cellular structure in Bénard convection. *Intl. J. Heat Mass Transfer* **13**, 849–856.

KELLY, R. E. & PAL, D. 1978 Thermal convection with spatiality periodic boundary conditions: resonant wavelength excitation. *J. Fluid Mech.* **86**, 433–456.

KERRISK, J. F. & KELLER, W. E. 1969 Thermal conductivity of fluid ^{3}He and ^{4}He at temperatures between 1.5 and 4.0 K and for pressures up to 34 atmospheres. *Phys. Rev.* **177**, 341–351.

KIRCHARTZ, K. R., MÜLLER, U., OERTEL, H. & ZIEREP, J. 1981 Axisymmetric and non-axisymmetric convection in a cylindrical container. *Acta Mechanica* **40**, 181–194.

KOSCHMIEDER, E. L. & PALLAS, S. G. 1974 Heat transfer through a shallow, horizontal convecting fluid layer. *Intl. J. Heat Mass Transfer* **17**, 991–1002.

LIBCHABER, A. & MAURER, J. 1978 Local probe in a Rayleigh–Bénard experiment in liquid helium. *J. Phys. Paris Lett.* **39**, L369–L372.

LIBCHABER, A. & MAURER, J. 1980 Une experience de Rayleigh–Bénard de géometrie reduite: multiplication, accrochage et démultiplication de fréquences. *J. Phys. Paris Colloq.* **3**, C41–C51.

MAURER, J. & LIBCHABER, A. 1979 Rayleigh–Bénard experiment in liquid helium: frequency locking and the onset of turbulence. *J. Phys. Paris Lett.* **40**, L419–422.

MAURER, J. & LIBCHABER, A. 1980 Effect of the Prandtl number on the onset of turbulence in liquid ^{4}He. *J. Phys Paris Lett.* **41**, 515–518.

MUELLER, K. H., AHLERS, G. & POBELL, F. 1976 Thermal expansion coefficient, scaling and universality near the superfluid transition of ^{4}He. *Phys. Rev.* B **14**, 2096–2118.

NEWELL, A. C. & WHITEHEAD, J. A. 1969 Finite-bandwidth, finite amplitude convection. *J. Fluid Mech.* **38**, 279–303.

OBERBECK, A. 1879 Uber die Warmeleitung der Flussigkeiten bei der Berucksichtigung der Stromungen infolge von Temperatur-Differenzen. *Ann. Phys. Chem.* **7**, 271–292.

PFOTENHAUER, J. M. 1984 The influence of rotation on the stability and heat transfer of Bénard convection in helium – I. Ph.D. dissertation University of Oregon, Eugene, OR, USA.

PFOTENHAUER, J. M. & DONNELLY, R. J. 1985 Heat transfer in liquid helium. *Adv. Heat Trans.* **17**, 65–158.

PFOTENHAUER, J. M., LUCAS, P. G. J. & DONNELLY, R. J. 1984 Stability and heat transfer of rotating cryogens. Part 2. Effects of rotation on heat-transfer and properties of convection in liquid ^{4}He. *J. Fluid Mech.* **145**, 239–252.

POCHEAU, A., CROQUETTE, V. & LE GAL, P. 1985 Turbulence in a cylindrical container near threshold. *Phys. Rev. Lett.* **55**, 1095.

SCHLÜTER, A., LORTZ, D. & BUSSE, F. 1965 On the stability of steady finite amplitude convection. *J. Fluid Mech.* **23**, 129–144.

SEGEL, L. A. 1969 Distant side-walls cause slow amplitude modulation of cellular convection. *J. Fluid Mech.* **38**, 203–224.

SHAUMEYER, J. N. & BEHRINGER, R. P. 1986 Unexpected observation in measurements of transport coefficients in ^{3}He–^{4}He mixtures near T_λ. *Phys. Rev.* B **33**, 3553–3555.

SOMERSCALES, E. F. C. & DOUGHERTY, T. S. 1970 Observed flow patterns at the initiation of convection in a horizontal liquid layer heated from below. *J. Fluid Mech.* **42**, 755–768.

STORK, K. & MÜLLER, U. 1975 Convection in boxes: an experimental investigation in vertical cylinders and annuli. *J. Fluid Mech.* **71**, 231–240.

SYDORIAK, S. G., SHERMAN, R. H. & ROBERTS, T. R. 1964 The T_{62} ^{3}He temperature scale. *Natur. Bur. Stand. J. Res.* **68A**, 547–579.

WALDEN, R. W. & AHLERS, G. 1981 Non-Boussinesq and penetrative convection in a cylindrical cell. *J. Fluid Mech.* **109**, 89–114.